J|A|C|S
ARTICLES
Published on Web 09/19/2002

The Structure of Self-Assembled Multilayers with Polyoxometalate Nanoclusters

Shaoqin Liu,[†] Dirk G. Kurth,*[,†] Bjoern Bredenkötter,[‡] and Dirk Volkmer*[,‡]

Contribution from the Max Planck Institute of Colloids and Interfaces, D-14424 Potsdam, Germany, and Department of Inorganic Chemistry 1, University of Bielefeld, P.O. Box 100 131, D-33501 Bielefeld, Germany

Received May 17, 2002

Abstract: Using electrostatic layer-by-layer self-assembly (ELSA), the formation of multilayers with polyelectrolytes and nanoscopic polyoxometalate (POM) clusters of different sizes and charges is investigated. The multilayers are characterized by UV−vis absorption spectroscopy, optical ellipsometry, cyclic voltammetry, and atomic force microscopy. In all cases, it is possible to find experimental conditions to achieve irreversible adsorption and regular multilayer deposition. Most importantly, the surface coverage is directly related to the total charge of the POM anion and can be controlled from submonolayer to multilayer coverage by adjusting the ionic strength of the dipping solutions. Imaging the interfaces after POM deposition by atomic force microscopy reveals a granular surface texture with nanometer-sized features. The average interfacial roughness amounts to approximately 1 nm. Cyclic voltammetry indicates that the electrochemical properties of the POM clusters are fully maintained in the polyelectrolyte matrix, which opens a route toward practical applications such as sensors or heterogeneous catalysts. Moreover, the permeability toward electrochemically active probe molecules can be tailored through the multilayer architecture and deposition conditions. Finally, we note that despite the low total charge and comparably small size of the discrete POM anions, the multilayers are remarkably stable. This work provides basic guidelines for the assembly of POM-containing ELSA multilayers and provides detailed insight into characteristic surface coverage, permeability, and electrochemical properties.

Introduction

Transition metal polyoxometalates (POMs) represent a well-known class of structurally well-defined clusters with an enormous variation in size, metal−oxygen framework topology, composition, and function. The preparation of POMs is based on the programmed self-assembly of metal oxide building blocks, which results in discrete, structurally uniform, nanoscopic clusters. A most attractive feature of POMs is the size dependence of their physicochemical properties. Most notable is the size-dependent propensity of the metal−oxygen framework to accommodate excess electrons.[1] The reduction process is reversible and occurs with marginal structural rearrangement. The rich redox chemistry of POMs is the basis for many catalytic processes.[2] Moreover, the reduced clusters frequently display a deep blue color, which leads to the general name "poly blue", or "heteropoly blue" if the framework includes heteroatoms. The ability of POMs to accept electrons under alteration of the optical properties can be used for the construction of functional electrooptical materials.[3] While the extinction coefficients of reduced POMs are comparable to those of organic dyes, the photochemical stability of reduced POMs is far superior to that of organic molecules.[4]

Although the number of functional POM compounds is steadily increasing, progress in POM synthesis has not been paralleled by a concomitant development of POM-based functional materials and devices. The realization of POM-based materials will require new methods to combine, position, and orient the clusters in the device architecture.[5] The exploitation and the encoding of value-adding properties in POM-based devices and materials remain elusive, mainly because these materials are obtained as crystalline solids that are hard to process. Due to the high lattice energies associated with crystallization, distinct mesoscopic supramolecular architectures, such as liquid crystalline phases, are also rarely observed.[6] Therefore, the next challenge in POM chemistry lies in developing methodologies to implement the clusters into well-defined, tailor-made architectures. To support, handle, manipulate, and operate such devices and materials, it will be necessary to collect and arrange the components in surface structures,[7] yet to date there are no generic methodologies available to do that. POMs can be adsorbed from an aqueous subphase to

* Corresponding author. Tel.: 0049-331-5679211. Fax: 0049-331-5679202. E-mail: kurth@mpikg-golm.mpg.de.
[†] Max Planck Institute of Colloids and Interfaces.
[‡] University of Bielefeld.

(1) (a) Pope, M. T. In *Mixed Valence Compounds*; Brown, D. B., Ed.; D. Reidel: Dordrecht, 1980; p 365. (b) Pope, M. T. *Prog. Inorg. Chem.* **1991**, *39*, 181.
(2) (a) Weinstock, I. A. *Chem. Rev.* **1998**, *98*, 113. (b) Sadakane, M.; Steckhan, E. *Chem. Rev.* **1998**, *98*, 219.
(3) (a) Liu, S.; Kurth, D. G.; Möhwald, H.; Volkmer, D. *Adv. Mater.* **2002**, *14*, 225. (b) Moriguchi, I.; Fendler, J. H. *Chem. Mater.* **1998**, *10*, 2205.
(4) Yamase, T. *Chem. Rev.* **1998**, *98*, 307.
(5) Kurth, D. G.; Volkmer, D. In *Polyoxometalate Chemistry*; Pope, M. T., Müller, A., Eds.; Kluwer: Dordrecht, 2001; pp 301−318.
(6) Polarz, S.; Smarsly, B.; Antonietti, M. *Chem. Phys. Chem.* **2001**, *1*, 457.

Langmuir monolayers of amphiphilic molecules at the air−water interface.[8] Thin films can be prepared by transferring these layers onto solid substrates with the Langmuir−Blodgett (LB) technique. While the LB method provides extensive control of structure and function, the resulting LB films are generally not very stable. In addition, this approach requires specialized equipment. Well-defined monolayers can be prepared by self-assembling the POM clusters directly onto certain metal surfaces.[9] While this approach is simple and applies to arbitrary substrate geometries, it is generally limited to certain clusters and metal surfaces. Also, the effect of chemisorption on the properties of the adsorbed clusters has still to be examined. To overcome the lattice energies associated with crystallization, it will be necessary to amend the surface chemical properties of the clusters. An elegant approach toward this goal relies on the exchange of the counterions of the POM anion with suitable surfactants.[10] The resulting surfactant-encapsulated clusters (SECs) are attractive building blocks because they combine the physicochemical properties of the inorganic POM core with the diverse assets of surface-active organic compounds, including solubility, wetting, and adhesion as well as biocompatibility.[11] Well-ordered thin films of SECs are readily prepared by the LB technique, spin coating, or evaporative methods.[12] Surfactants as structural components can also induce new distinct noncrystalline phases such as technologically important liquid crystals.

The electrostatic layer-by-layer self-assembly (ELSA) method is one of the most promising new methods for thin-film fabrication and has been successfully applied to charged organic polymers,[13] nanoparticles, and other inorganic materials.[14,15] Its simplicity and versatility in combination with high quality and uniform coatings opens broad perspectives in both fundamental and applied research. This method rests on the alternating deposition of oppositely charged species on the substrate surface, and film formation is primarily attributed to electrostatic interactions and van der Waals forces.[16,17] This approach offers thickness control at the nanometer level and can be applied to arbitrarily shaped objects; it also permits co-assembly with different functional components, and the deposition process is readily automated. While the resulting multilayers are robust and permeable, the internal structure is typically not stratified due to interpenetration of adjacent layers.[18] Recently, the ELSA method has been adapted to the immobilization of POM anions.[19] However, little is known about the fundamental principles of this seemingly straightforward procedure. Due to their discrete and uniform structure and charge, POMs are unique model systems to study fundamental questions in multilayer assembly. Moreover, we can address questions concerning environmental effects on the function by investigating changes in the physicochemical properties of the immobilized POM clusters, including electrochemistry, fluorescence, and optical absorption.[20] To learn more about the assembly of these systems, we present a detailed investigation on multilayer assemblies with POM clusters of different sizes and charges (Chart 1) and discuss some of the guiding principles for the deposition of POM anions in multilayers with respect to layer architecture, surface coverage, permeability, and electrochemistry.

Experimental Section

Materials. $(NH_4)_{14}[Na(H_2O)P_5W_{30}O_{110}]$, $(NH_4)_{11.5}K_{0.5}[Eu(H_2O)P_5W_{30}O_{110}]$, and $Na_{16}[Co_4(H_2O)_2P_4W_{30}O_{112}]$ were prepared according to literature procedures.[21] The crystal structures of the Preyssler and Finke-type POMs were reported in the literature.[22]

Crystal Structure Determination. Brown-green crystal platelets of Co−POM were obtained by slow recrystallization from saturated aqueous NaCl solution after refluxing. A single crystal of Co−POM was removed from the mother liquor and immediately cooled to 183(2) K on a Bruker AXS SMART diffractometer (three-circle goniometer with 1K CCD detector, Mo Kα radiation, graphite monochromator; full-sphere data collection in ω at 0.3° scan width in four runs with 606, 500, 606, and 500 frames ($\Phi = 0$, 88, 180, and 268°) at a detector distance of 5 cm). A total of 34 431 reflections ($1.68 < \Theta < 27.02°$) were collected, of which 15 648 unique reflections (R(int) = 0.0365) were used. An empirical absorption correction using equivalent reflections was performed with the program SADABS. A summary of the crystallographic data and refinement parameters is provided in the

(7) Swalen, J. D.; Allara, D. L.; Andrade, J. D.; Chandross, E. A.; Garoff, S.; Israelachvili, J.; McCarthy, T. J.; Murray, R.; Pease, R. F.; Rabolt, J. F.; Wynne, K. J.; Yu, H. *Langmuir* **1987**, *3*, 932.
(8) Clemente-Léon, M.; Mingotaud, C.; Agricole, B.; Gomez-Garcia, C. J.; Coronado, E.; Delhaes, P. *Angew. Chem., Int. Ed. Engl.* **1997**, *36*, 1114.
(9) Klemperer, W. G.; Wall, C. G. *Chem. Rev.* **1998**, *98*, 297.
(10) Kurth, D. G.; Lehmann, P.; Volkmer, D.; Cölfen, H.; Müller, A.; Du Chesne, A. *Chem. Eur. J.* **2000**, *6*, 385.
(11) Kurth, D. G.; Lehmann, P.; Volkmer, D.; Müller, A.; Schwahn, D. *J. Chem. Soc., Dalton Trans.* **2000**, 3989.
(12) Volkmer, D.; Du Chesne, A.; Kurth, D. G.; Schnablegger, H.; Lehmann, P.; Koop, M. J.; Müller, A. *J. Am. Chem. Soc.* **2000**, *122*, 1995.
(13) (a) Decher, G.; Hong, J. D. *Ber. Bunsen-Ges. Phys. Chem. Chem.* **1991**, *95*, 1430. (b) Decher, G. *Science* **1997**, *277*, 1232. (c) Decher, G.; Hong, J. D. *Thin Solid Films* **1992**, *210/211*, 831. (d) Stockton, W. B.; Rubner, M. F. *Macromolecules* **1997**, *30*, 2717. (e) Decher, G. In *Templating, Self-organization*; Sauvage, J. P., Hossein, M. W., Eds.; Comprehensive Supramolecular Chemistry 9; Pergamon Press: Oxford, 1996; p 507. (f) Ferreira, M.; Cheung, J. H.; Rubner, M. F. *Thin Solid Films* **1994**, *244*, 807. (g) Cheung, J. H.; Fou, A. C.; Rubner, M. F. *Macromolecules* **1995**, *28*, 7115. (h) Fou, A. C.; Onitsuka, O.; Ferrira, M.; Rubner, M. F. *Mater. Res. Soc. Symp. Proc.* **1995**, *369*, 575. (i) Harris, J. J.; DeRose, P. H.; Bruening, M. L. *J. Am. Chem. Soc.* **1999**, *121*, 1978. (j) Sullivan, D. M.; Brueing, M. L. *J. Am. Chem. Soc.* **2001**, *123*, 11805.
(14) (a) Kotov, N. A.; Dekany, I.; Fendler, J. H. *J. Phys. Chem.* **1995**, *99*, 13065. (b) Schmitt, J.; Decher, G.; Dressick, W. J.; Brandow, S. L.; Geer, R. E.; Shashidhar, R.; Calvert, J. M. *Adv. Mater.* **1997**, *9*, 61. (c) Fendler, J. H.; Meldrum, F. C. *Adv. Mater.* **1995**, *7*, 607. (d) Gao, M.; Gao, M.; Zhang, X.; Yang, Y.; Yang, B.; Shen, J. *J. Chem. Soc., Chem. Commun.* **1994**, 2777. (e) Gao, M.; Richter, B.; Kirstein, S. *Adv. Mater.* **1997**, *9*, 802. (f) Ariga, K.; Lvov, Y.; Onda, M.; Ichinose, I.; Kunitake, T. *Chem. Lett.* **1997**, 125. (g) Feldheim, D. L.; Grabar, K. C.; Natan, M. J.; Mallouk, T. E. *J. Am. Chem. Soc.* **1996**, *118*, 7640. (h) Kleinfeld, E. R.; Ferguson, G. S. *Science* **1994**, *265*, 370.
(15) (a) Feldheim, D. L.; Grabar, K. C.; Natan, M. J.; Mallouk, T. E. *J. Am. Chem. Soc.* **1996**, *118*, 7640. (b) Kleinfeld, E. R.; Ferguson, G. S. *Science* **1994**, *265*, 370. (c) Bell, C. M.; Arendt, M. F.; Gomez, L.; Schnehl, R. H.; Mallouk, T. E. *J. Am. Chem. Soc.* **1994**, *116*, 8374. (d) Cassagneau, T.; Mallouk, T. E.; Fendler, J. H. *J. Am. Chem. Soc.* **1998**, *120*, 8374. (e) Keller, S. W.; Kim, H. N.; Mallouk, T. E. *J. Am. Chem. Soc.* **1994**, *116*, 8817. (f) Kovtyukhova, N. I.; Ollivier, P. J.; Martin, B. R.; Mallouk, T. E.; Chizhik, A. A.; Buzaneva, E. V.; Gorchinskiy, A. D. *Chem. Mater.* **1999**, *11*, 771. (g) Kaschak, D. M.; Mallouk, T. E. *J. Am. Chem. Soc.* **1996**, *118*, 4222.
(16) Decher, G. *Science* **1997**, *277*, 1232.
(17) (a) Kotov, N. A. *Nanostruct. Mater.* **1999**, *12*, 789. (b) Dubas, S. T.; Schlenoff, J. B. *Macromolecules* **1999**, *32*, 8153.
(18) (a) Lvov, Y.; Decher, G.; Haas, H.; Möhwald, H.; Kalachev, A. *Phys. Status Solidi B* **1994**, *198*, 89. (b) Decher, G.; Lvov, Y.; Schmitt, J. *Thin Solid Films* **1998**, *244*, 772.
(19) (a) Ichinose, I.; Tagawa, H.; Mizuki, S.; Lvov, Y.; Kunitake, T. *Langmuir* **1998**, *14*, 187. (b) Moriguchi, I.; Fendler, J. H. *Chem. Mater.* **1998**, *10*, 2205. (c) Caruso, F.; Kurth, D. G.; Volkmer, D.; Koop, M. J.; Müller, A. *Langmuir* **1998**, *14*, 3462. (d) Kurth, D. G.; Volkmer, D.; Kuttorf, M.; Müller, A. *Chem. Mater.* **2000**, *12*, 2829. (e) Ingersoll, D.; Kulesza, P. J.; Faulkner, L. R. *J. Electrochem. Soc.* **1994**, *141*, 140. (f) Kuhn, A.; Anson, F. C. *Langmuir* **1996**, *12*, 5481. (g) Sun, S.; Zhang, J. *Electrochim. Acta* **1998**, *43*, 943. (h) Bange, K.; Gambke, T. *Adv. Mater.* **1990**, *2*, 10.
(20) Liu, S.; Kurth, D. G.; Volkmer, D. *Chem. Commun.* **2002**, 965.
(21) (a) Dickman, M. H.; Gama, G. J.; Kim, K. C.; Pope, M. T. *J. Cluster Sci.* **1996**, *7*, 551. (b) Creaser, I.; Heckel, M. C.; Neitz, R. J.; Pope, M. T. *Inorg. Chem.* **1993**, *32*, 1573. (c) Finke, R. G.; Droege, M. W. *Inorg. Chem.* **1983**, *22*, 1006.
(22) (a) Alizadeh, M. H.; Harmalker, S. P.; Jeannin, Y.; Martin-Frère, J.; Pope, M. T. *J. Am. Chem. Soc.* **1985**, *107*, 2662. (b) Weakley, T. J. R.; Finke, R. G. *Inorg. Chem.* **1990**, *29*, 1235.

Chart 1. (Top) Coordination Polyhedra Representation of POM Clusters Used in This Study[a] and
(Bottom) Schematic Illustration of the ELSA Films Assembled with Negatively Charged Nanoscopic POM Clusters (Polygons) and Macromolecular Polyelectrolytes[b]

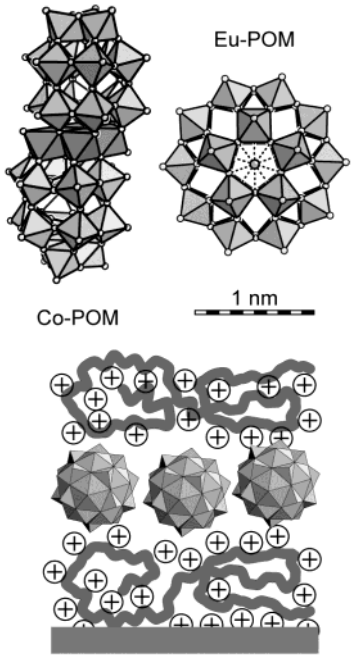

[a] Abbreviations: Co−POM, $[Co_4(H_2O)_2P_4W_{30}O_{112}]^{16-}$; Na−POM, $[Na(H_2O)P_5W_{30}O_{110}]^{14-}$; Eu−POM, $[Eu(H_2O)P_5W_{30}O_{110}]^{12-}$. The Eu− and Na−POMs are isostructural but differ in the total charge. [b] The packing density of the POMs, the film architecture, and the permeability of the multilayers are readily controlled through the assembly conditions.

Supporting Information. The structure was solved by direct methods with the program SHELXS-97 and refined by full-matrix least-squares based on F^2 using SHELXL-97 to give a final $R = 0.0355$ for 12 836 reflections with $I > 2\sigma(I)$.[23] Atoms of the polyoxometalate anion and sodium counterions were refined anisotropically, while the residual oxygen atoms were refined isotropically. No attempts were undertaken to locate or to calculate hydrogen atom positions. As usual in crystal structures containing large polyoxometalates, some countercation positions were slightly disordered and only partially occupied. Further information, like positional and thermal parameters, can be found in the Supporting Information.

Multilayer Preparation. Quartz, silicon, and ITO-coated glass (one-sided, ca. 6 Ωm, 7 mm × 50 mm) substrates were cleaned according to literature procedures.[24] Poly(ethylenimine) (PEI, MW 50 000, Aldrich, 10^{-2} mol/L) was adsorbed by immersing the substrates into the solution for 20 min, rinsing with water, and drying under an Ar flow. POM/polyelectrolyte multilayers were prepared by first depositing poly(styrenesulfonate) (PSS, MW 70 000, Aldrich) and poly(allylamine hydrochloride) (PAH, MW 8 000−11 000, Aldrich) onto the PEI-modified substrate. These polyelectrolyte layers were deposited from 10^{-3} mol/L aqueous solutions (pH 5−6), using an immersion time of 10 min, followed by rinsing with water and drying after each second layer. POMs were adsorbed from aqueous solution (5×10^{-4} mol/L, pH 5−6) using an immersion time of 10 min. The ionic strength of the solutions was adjusted with NaCl as mentioned in the text.

Instrumentation. UV−vis spectra were recorded with a Varian Cary 50 after each layer deposition. Ellipsometric measurements on silicon substrates were performed with null ellipsometry using a Multiskop (Optrel Germany, 2 mW HeNe laser, $\lambda = 632.8$ nm; angle of incidence 70°). The refractive index of the multilayer was determined from a thick sample. This value was then used for the thickness calculation of thin layers. Cyclic voltammetry was carried out in a three-electrode cell: ITO-coated glass electrode (1.05 cm^2) as the working electrode, platinum foil as the counter electrode, and an Ag/AgCl/KCl (3 mol/L) reference electrode. Before assembly, the cleaned ITO-coated glass electrodes were functionalized with (3-aminopropyl)trimethoxysilane to yield an amine-functionalized surface.[25] AFM measurements were performed in air with a Nanoscope IIIa (Digital Instruments Inc., Santa Barbara, CA) operating in the tapping mode (TM). TESP silicon tips with a cantilever length of 125 μm and a resonance frequency of 300−330 kHz were employed.

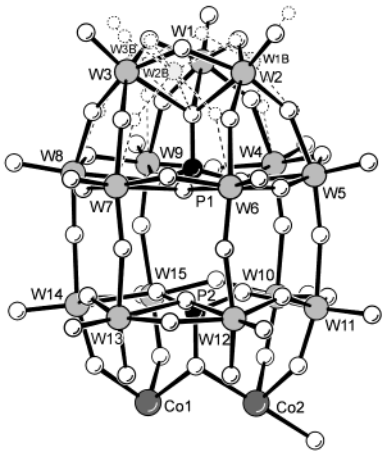

Figure 1. Ball-and-stick representation of half of the $[Co_4(H_2O)_2P_4W_{30}O_{112}]^{16-}$ (Co−POM) anion including the labeling scheme. The broken sticks/balls belong to a W_3O_{12} capping unit, which is rotated by ∼60° around the C_3 symmetry axis of the trivacant $[P_2W_{15}O_{56}]^{12-}$ unit.

Results and Discussion

First we will discuss the crystal structure of $Na_{16}[Co_4(H_2O)_2(P_2W_{15}O_{56})_2]\cdot 60H_2O$, and then we will describe the results on multilayer assembly. The crystal structure of this compound is solved and presented in order to complete the available analytical data of this compound, the synthesis of which was reported previously.[26] The sandwich-type $[Co_4(H_2O)_2(P_2W_{15}O_{56})_2]^{16-}$ anion consists of two lacunary α-B-$[P_2W_{15}O_{56}]^{12-}$ ligands, which coordinate a central tetranuclear metal cluster consisting of edge-sharing CoO_6 octahedra. During the course of the crystal structure refinement, it became apparent that the asymmetric unit contains a statistical mixture of the main POM isomer (ca. 89%) described below, and a second isomer where the terminal W_3O_{12} capping unit is rotated by ∼60° around the C_3 symmetry axis of the trivacant $[P_2W_{15}O_{56}]^{12-}$ unit (Figure 1).[27]

The single-crystal X-ray structures of isostructural $[M_4(H_2O)_2(P_2W_{15}O_{56})_2]^{n-}$ POM anions containing M = Cu(II),[28] Zn,[29] Mn(II),[30] and Fe(III)[31] have been reported in the literature. The Co−POM cluster shows the expected geometrical features of

(23) Sheldrick, G. M. SHELXS/L/H, SADABS; University of Göttingen, 1997.
(24) (a) Kern, W. *RCA Eng.* **1983**, *28*, 99. (b) Philips, B. F. *J. Vac. Sci. Technol. A* **1983**, *A1*, 646. (c) Kern, W. *Semicond. Int.* **1984**, 94.
(25) (a) Kurth, D. G.; Bein, T. *Langmuir* **1995**, *11*, 3061. (b) Evenson, S. A.; Badyal, J. P. S.; Pearson, C.; Petty, M. C. *J. Phys. Chem.* **1996**, *100*, 11672.
(26) Finke, R. G.; Droege, M. W.; Domaille, P. J. *Inorg. Chem.* **1987**, *26*, 3886.
(27) The presence of different polymetalate isomers is probably due to incomplete separation of the α- and β-$P_2W_{18}O_{62}^{6-}$ used as starting material. The single crystals thus contain four different polymetalate isomers, which derive from statistical combination of lacunary α- and β-B-$P_2W_{15}O_{56}^{12-}$ ligands in the sandwich-type polymetalate.
(28) Weakley, T. J. R.; Finke, R. G. *Inorg. Chem.* **1990**, *29*, 1235.
(29) Finke, R. G.; Weakley, T. J. R. *J. Chem. Crystallogr.* **1994**, *24*, 123.
(30) Gómez-García, C. J.; Borrás-Almenar, J. J.; Coronado, E.; Ouahab, L. *Inorg. Chem.* **1994**, *33*, 4016.
(31) Zhang, X.; Chen, Q.; Duncan, D. C.; Campana, C. F.; Hill, C. L. *Inorg. Chem.* **1997**, *36*, 4208.

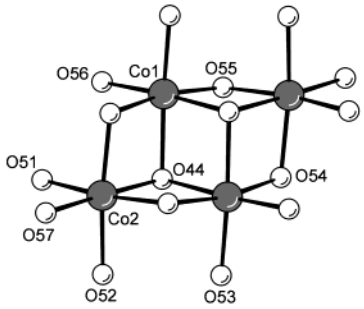

Figure 2. Ball-and-stick representation of the central tetranuclear Co_4O_{16} unit.

trivacant Wells−Dawson units. The average W−O bond distances (W−$O_{terminal}$, 1.723(7) Å; W−$O_{\mu 2-bridging}$, 1.924(70) Å; W−$O_{\mu 3-bridging}$, 2.357(17) Å; W−$O_{\mu 4-bridging}$, 2.373(18) Å) and the average P−O bond distance (P−O, 1.544(19) Å) are, within standard deviation, identical to the corresponding values of the Mn(II) and Fe(III) derivatives. The central tetranuclear Co_4O_{16} unit contains four high-spin Co(II) ions, which are situated in a slightly distorted octahedral coordination environment (Figure 2). The average Co−O bond distance amounts to 2.094(50) Å; the metal−oxygen bond distance for the coordinated H_2O ligand shows no significant bond elongation (Co(2)−O(57), 2.103(7) Å), in contrast to the isostructural Cu(II) compound, where the corresponding copper−oxygen bond distance is 2.61(4) Å[28] owing to the huge Jahn−Teller distortion of the CuO_6 group. The central four cobalt atoms lie in the same plane; the nonbonding distances of the rhomb-like arrangement of Co ions amount to 3.175(1) and 3.153(1) Å, respectively.

It should be noted here that the amount of crystal water molecules (60) found here is significantly larger than the reported literature values for the sodium salts of the Zn, Mn, and Cu derivatives (ranging from 50 to 53). The most important parameters of the crystal structure are summarized in Table 1. Further information, such as complete lists of positional and thermal parameters, packing diagrams, and labeling schemes, are provided in the Supporting Information.

Electrostatic layer-by-layer self-assembly of POM anions is monitored by UV−vis absorption spectroscopy and optical ellipsometry. In the following we will focus on Eu−POM-based multilayers. Figure 3 shows UV−vis spectra of PEI/PSS/PAH-(Eu−POM/PAH)$_m$ multilayers. Both the Eu−POM and PAH dipping solutions do not contain NaCl. The absorbance in the wavelength range of 200−400 nm increases steadily with the number of layers, *m*, which confirms irreversible adsorption of Eu−POM and PAH. We note that the absorbance of Eu−POM measured after rinsing the layer and after deposition of the next PAH layer remains nearly constant. Regular layer growth is revealed by a linear dependence of the absorbance determined at two different wavelengths (202 and 282 nm) versus the number of layers, *m*. In each deposition step, an equal amount of Eu−POM is adsorbed at the interface, as indicated by the straight line and the zero intercept. The absorbance band at 282 nm is attributed to Eu−POM, while the band at 202 nm arises from both PSS and Eu−POM. Therefore, the contribution of PSS in the precursor layer to the absorbance at 202 nm results in a nonzero intercept. From the UV−vis spectra, the surface coverage per layer, Γ, of Eu−POM can be calculated by

$$\Gamma = (N_A A_\lambda)/2m\epsilon_\lambda$$

Table 1. Crystal Structure Data of $Na_{16}[Co_4(H_2O)_2(P_2W_{15}O_{56})_2]\cdot 60H_2O$ (Co−POM)

formula	$H_{128}Co_4Na_{16}O_{174}P_4W_{30}$
formula weight (*M*), g mol^{-1}	9155.96
crystal size, mm^3	0.04 × 0.20 × 0.25
crystal color/habit	green-brown/plate
crystal system	triclinic
space group	$P\bar{1}$ (No. 2)
a, Å	13.6284(8)
b, Å	13.8525(8)
c, Å	22.823(1)
α, deg	89.906(1)
β, deg	78.302(1)
γ, deg	61.571(1)
V, Å^3	3687.9(4)
Z	1
ρ_{calcd}, g cm^{-3}	4.123
μ, mm^{-1}	23.951
F(000)	4084
T, K	183(2)
2*θ* range	3.36° < 2*θ* < 54.04°
reflections collected	34 431
independent reflections	15 648 [*R*(int) = 0.0365]
GOF on F^2	1.030
R (>2*σ*(*I*))	$R_1{}^a = 0.0355$ wR_2 = 0.0896
R (all data)	$R_1{}^a = 0.0478$ wR_2 = 0.0945
$(\Delta/\rho)_{max}$, e$^-$/Å^3	2.793
$(\Delta/\rho)_{min}$, e$^-$/Å^3	−2.406

^{a} $R_1 = \sum||F_o| - |F_c||/\sum|F_o|$. ^{b} w$R_2 = [\sum w(F_o^2 - F_c^2)^2/\sum(F_o^4)]^{1/2}$. $w_1 = 1/[\sigma^2(F_o^2) + (0.0394P)^2 + 47.2275P]$.

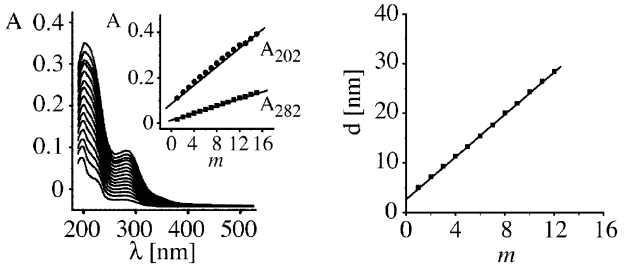

Figure 3. (Left) UV−vis absorption spectra of (Eu−POM/PAH)$_m$ multilayers for $m = 1-12$ adsorbed on a PEI/PSS/PAH precursor film. The inset shows the absorbance at 202 and 282 nm as a function of *m*. (Right) Film thickness of the multilayers determined by ellipsometry. The thickness increment per (Eu−POM/PAH) layer pair is 2.1 nm. Multilayers are assembled from dipping solutions with no NaCl added.

where N_A is Avogadro's constant, A_λ is the absorbance, and ϵ_λ is the isotropic molar extinction coefficient ($\epsilon_{282} = 8.8 \times 10^4$ M^{-1} cm^{-2}) at wavelength λ (282 nm). The average surface coverage amounts to (2.8 ± 0.14) × 10^{13} Eu−POM anions/cm^2 or (4.7 ± 0.23) × 10^{-11} mol/cm^2, which corresponds to an average area of (3.6 ± 0.2) nm^2/anion. Compared to the packing of the crystalline solid, this value corresponds to submonolayer coverage. In the crystalline solid, a single Eu−POM cluster occupies a volume of 3.16 nm^3.[32] In the case of an isotropic orientation, the POM cluster can be treated as a spherically shaped object of that volume. Consequently, the surface area of the Eu−POM anion amounts to 2.6 nm^2. Therefore, the packing density of Eu−POM anions in the multilayer is approximately 0.72 times that of the crystalline material. This estimate provides an upper limit for the surface coverage because the volume of the unit cell includes the POM anion as well as

(32) Dickman, M. H.; Gama, G. J.; Kim, K.-C.; Pope, T. M. *J. Cluster Sci.* **1996**, *7*, 567.

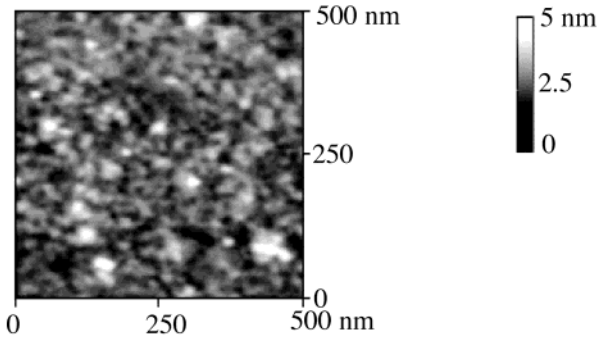

Figure 4. Representative AFM image of the PEI/PSS/PAH/Eu−POM interface.

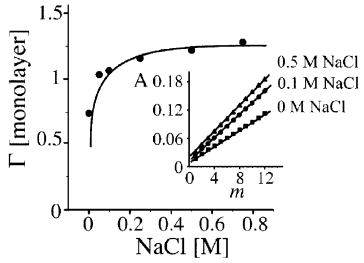

Figure 5. Surface coverage per layer, Γ, of Eu−POM in (Eu−POM/PAH)$_m$ multilayers as a function of the NaCl concentration of the Eu−POM solution. The surface coverage is based on the packing density in the crystalline solid. PAH is deposited from aqueous solution containing no NaCl. The inset shows the absorbance at 282 nm at different NaCl concentrations versus the number of layers, *m*, confirming linear multilayer growth.

counterions and hydration water. Nevertheless, this simplified analysis provides values similar to those obtained with sophisticated molecular modeling procedures.[33]

Measurements of the thickness of PEI/PSS/PAH(Eu−POM/PAH)$_m$ multilayers by optical ellipsometry (Figure 3) reveal that the thickness increases linearly with the number of layers, *m*, in agreement with the absorbance measurements. The average thickness increment of a (Eu−POM/PAH) layer pair is 2.1 nm. Because no salt is used during deposition, the PAH layer thickness is estimated to be approximately 1 nm.[34] From the size of the POM anion and the previously determined surface coverage, the thickness of the Eu−POM layers is estimated to be approximately 1 nm. Taken together, the overall thickness for a layer pair is estimated to be approximately 2 nm, in agreement with the experimentally determined value.

AFM imaging of the interfaces reveals subtle variations of the surface topology upon adsorption of PAH and Eu−POM. The PEI/PSS/PAH precursor layer, adsorbed on mica, shows a featureless surface topology, consistent with previously published results.[35] Upon adsorption of Eu−POM onto that layer, we observe a granular texture (Figure 4). The height variation of the texture is 1.5 nm, which corresponds approximately to the (average) size of the Eu−POM cluster. However, it is not possible to detect individual POM anions. The root-mean-square (RMS) value of the surface roughness is 0.4, 0.8, 1, and 1.9 nm for PEI/PSS/PAH/Eu−POM, PEI/PSS(PAH/Eu−POM)$_2$, PEI/PSS(PAH/Eu−POM)$_3$, and PEI/PSS(PAH/Eu−POM)$_5$, respectively. Finally, for a PEI/PSS(PAH/Eu−POM)$_{10}$ multilayer, the roughness converges to a constant value of 0.9 nm. Likewise, the features of the interface texture become larger. We like to attribute the appearance of a granular texture to the following effects. Due to the submonolayer coverage and the nanoscopic size, adsorption of Eu−POM will cause an inhomogeneous charge pattern. In addition, the interaction of the anion with the underlying polyelectrolyte matrix may induce a local structural reorganization.[35] The initial increase in surface roughness for the first few layers is attributed to a substrate effect. After several deposition cycles, the polyelectrolyte partially anneals interfacial inhomogeneities and renders the surface virtually uniform so that overall multilayer growth is very regular. It is interesting to note that these multilayers do not show well-resolved Kiessig fringes in X-ray reflectometry.[36] Apparently, on the macroscopic length scale the roughness is much larger, and these multilayers are not as homogeneous as one would anticipate from the AFM images. Roughness on this length scale may be induced by loss of water, drying effects, and interfacial tension.

A possible explanation for the low surface coverage of Eu−POM, as discussed in the previous section, could be ascribed to residual electrostatic or dipolar repulsions of adjacent cluster anions at the interface. By adding salt to the POM solution, it might be possible to screen the electrostatic repulsion, thus allowing the cluster anions to move together more closely. Figure 5 shows the surface coverage per layer as a function of the NaCl concentration of the POM dipping solution. Here and in the following, the surface coverage is reported as number of monolayers based on the packing density in the crystalline solid. PAH is deposited from salt-free solution. As one can see, the surface coverage per deposition step increases in a nonlinear way upon addition of NaCl to the dipping solution, while multilayer growth remains linear (inset). A plateau is reached when the NaCl concentration exceeds 0.1 M. The average surface coverage per layer at a NaCl concentration of 0.1 M is $(4.1 \pm 0.2) \times 10^{13}$ anions/cm^2 or $(6.8 \pm 0.34) \times 10^{-11}$ mol/cm^2, which corresponds to an average area of (2.4 ± 0.12) nm^2/anion. This surface coverage is akin to the packing density in the crystalline solid (2.6 nm^2, vide supra) and, therefore, corresponds to a monolayer. It is interesting to note that if NaCl concentration exceeds 1 M, regular film formation may fail. This behavior is in contrast to polyelectrolytes that still adsorb under these conditions.[37] In the following examples, we therefore chose to assemble multilayers from POM solutions with a NaCl concentration of 0.1 M. Here, too, we do not observe well-resolved Kiessig fringes in X-ray reflectometry.

In addition, we note that the Eu−POM surface coverage depends on the ionic strength of the polyelectrolyte dipping solution. Figure 6 shows the surface coverage of (Eu−POM/PAH)$_m$ multilayers as a function of the NaCl concentration of the PAH solution. Obviously, the amount of POM anions adsorbed increases as NaCl is added to the PAH dipping solution. At a NaCl concentration of 0.5 M, the surface coverage per layer is $(1.0 \pm 0.05) \times 10^{14}$ anions/cm^2 or $(1.7 \pm 0.08) \times$

(33) Modeling the solvent-accessible surface of a 0.14 nm probe (see ref 12) provides a volume of 3.29 nm^3 or a surface area of 2.67 nm^2 (unpublished results).

(34) (a) Schmitt, J.; Grünewald, T.; Kjaer, K.; Pershan, P.; Decher, G.; Lösche, M. *Macromolecules* **1993**, *26*, 7058. (b) Decher, G.; Schmitt, J. *Prog. Colloid Polym. Sci.* **1992**, *89*, 160.

(35) Kotov, N. A.; Dekang, I.; Fendler, J. H. *J. Phys. Chem.* **1995**, *99*, 13065.

(36) Computing the reflectance shows that Kiessig fringes disappear if the Gaussian roughness of the outer interface exceeds 5 nm (Russell, T. P. *Mater. Sci. Rep.* **1990**, *5*, 171). In AFM, we observe total height variations of 5−8 nm, which are most likely responsible for the loss of coherent interference in X-ray reflectometry.

(37) Decher, G.; Hong, J. D.; Schmitt, J. *Thin Solid Films* **1992**, *210/211*, 831.

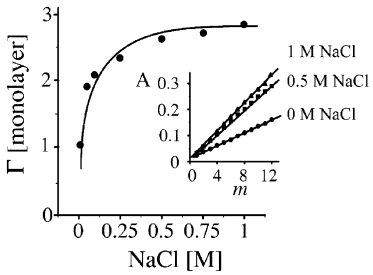

Figure 6. Surface coverage per layer, Γ, of Eu−POM in $(Eu-POM/PAH)_m$ multilayers as a function of the NaCl concentration of the PAH dipping solution. The surface coverage is based on the packing density in the crystalline solid. Eu−POM is deposited from aqueous solution containing 0.1 M NaCl. The inset shows the absorbance at 282 nm at different NaCl concentrations versus the number of layers, *m*, confirming linear multilayer growth.

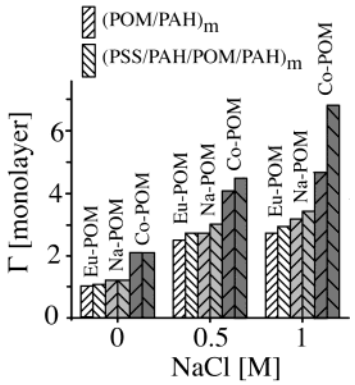

Figure 7. Surface coverage per layer, Γ, of Na−POM, Eu−POM and Co−POM in $(POM/PAH)_m$ and $(PSS/PAH/POM/PAH)_m$ multilayers as a function of NaCl concentration of the polyelectrolyte dipping solution. The surface coverage is based on the packing density in the crystalline solid. POMs are deposited from aqueous solution containing 0.1 M NaCl.

10^{-10} mol/cm^2, which corresponds to an average area of (1 ± 0.05) nm^2/anion. Apparently, more than one monolayer adsorbs on the PAH interface under these conditions, which we attribute to the following reasons. At high ionic strength, the polyelectrolyte adsorbs at the interface in a more condensed, coiled conformation.[38] We therefore propose that the rather small Eu−POM anion both adsorbs at the top of the PAH interface and also diffuses into the PAH layer, binding to internal sites of PAH through ion exchange of uncompensated chloride (or hydroxide) anions. At low ionic strength, PAH adapts a rather extended conformation and adsorbs at the surface like a flat pancake. Thus, the POM anions adsorb primarily at the top of the PAH interface. With AFM we also observe a granular texture; however, the features are larger compared to those of films prepared without salt. The surface roughness of these multilayers amounts to 0.4, 0.7, and 0.8 nm for $m = 1$, 2, and 3, respectively. Optical ellipsometry confirms regular growth of POM/PAH multilayers. Regular layer growth is observed for as many as 100 deposition cycles. The number of layers is large enough to defy any doubt that it will continue further in the same fashion. However, as in the previous cases and in the following ones, we do not observe well-resolved Kiessig fringes in X-ray reflectometry of these multilayers.

In the following, we will compare different layer architectures, namely (a) $(POM/PAH)_m$ and (b) $(PSS/PAH/POM/PAH)_m$ multilayers deposited on the PEI/PSS/PAH or PEI precursor layer, respectively. Figure 7 shows the POM surface coverage of the different multilayer architectures and different POMs as a function of the NaCl concentration of the polyelectrolyte dipping solution. The coverage is reported in number of monolayers based on the (average) packing density derived from the X-ray crystal structure analysis. Regular film growth is confirmed by UV−vis spectroscopy and optical ellipsometry in all cases. If no salt is added, we note that for both architectures the surface coverages of Eu−POM and Na−POM are almost identical, while it is approximately 20% larger for Co−POM. If the NaCl concentration is increased, the surface coverage of the anions becomes more differentiated. First, the surface coverage increases in all cases. As discussed in the previous section, this effect is attributed to changes in the conformation of the adsorbed polyelectrolyte as the salt concentration is increased. Second, in $(PSS/PAH/POM/PAH)_m$ multilayers, the surface coverage is a little higher than in $(POM/PAH)_m$ multilayers. In the case of Co−POM, this effect is considerably larger than with the Preyssler anions.

In a control experiment, $PEI(PSS/PAH)_mPSS$ multilayers are immersed into a Eu−POM or Co−POM dipping solution to verify if and to what extent the anions penetrate the multilayer. In contrast to the previous experiments, these multilayers are terminated by a negatively charged PSS layer to minimize interference by deposition at the top interface. While the PSS and POM solutions do not contain NaCl, the PAH solution is 0.5 M in NaCl. In this case, UV−vis spectroscopy also confirms the presence of POM anions, which we attribute to penetration of anions into the multilayer. The adsorption continues for approximately 1 h for Co−POM and 2 h in case of Eu−POM, after which we do not detect a further increase of the UV−vis absorbance. The total amount adsorbed in $PEI(PSS/PAH)_{10}PSS$ or $PEI(PSS/PAH)_5PSS$ amounts in both cases to approximately $(2.0 \pm 0.1) \times 10^{-10}$ mol/cm^2 for Eu−POM and $(2.7 \pm 0.14) \times 10^{-10}$ mol/cm^2 for Co−POM. This amount corresponds to the coverage typically achieved in one deposition step. The fact that the same amount of material is adsorbed in layers of different thicknesses indicates that the POM anions adsorb primarily at the top first layers of the interface. We therefore conclude that the slightly larger surface coverage in $(PSS/PAH/POM/PAH)_m$ multilayers is due to the intermittent PAH/PSS/PAH cushions.

Notably, the surface coverage decreases in the order Co−POM, Na−POM, and finally Eu−POM. For example, at a NaCl concentration of 1 M, the surface coverage per layer of Eu−POM is $(1.8 \pm 0.2) \times 10^{-10}$ mol/cm^2 for $(Eu-POM/PAH)_m$ and $(2.0 \pm 0.2) \times 10^{-10}$ mol/cm^2 for $(PSS/PAH/Eu-POM/PAH)_m$ multilayers, respectively. For Na−POM, the surface coverages are $(2.1 \pm 0.2) \times 10^{-10}$ mol/cm^2 for $(Na-POM/PAH)_m$ and $(2.3 \pm 0.2) \times 10^{-10}$ mol/cm^2 for $(PSS/PAH/Na-POM/PAH)_m$ multilayers, which are slightly larger than that for Eu−POM. However, there is a significant increase in the surface coverage per layer for Co−POM, namely $(2.9 \pm 0.3) \times 10^{-10}$ mol/cm^2 for $(Co-POM/PAH)_m$ and $(4.2 \pm 0.4) \times 10^{-10}$ mol/cm^2 for $(PSS/PAH/Co-POM/PAH)_m$ multilayers. Clearly, the trend in surface coverage is related to the charge of the anions: Co−POM (16), Na−POM (14), and Eu−POM (12). This result clearly demonstrates the importance of the total charge of the nanoparticle in ELSA deposition.[39]

(38) Knoll, W. *Curr. Opin. Colloid Interface Sci.* **1996**, *1*, 137.

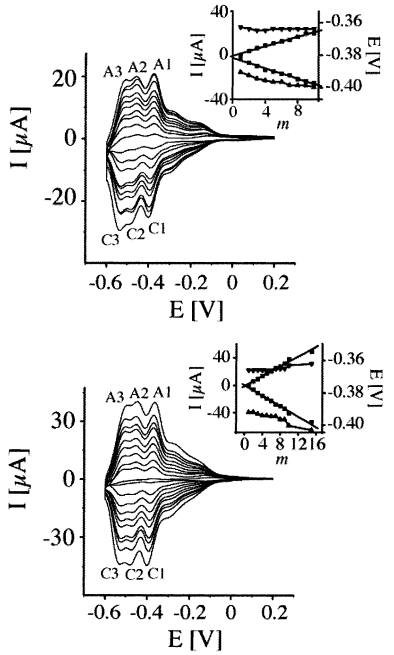

Figure 8. Cyclic voltammograms of $(Eu-POM/PAH)_m$ (top) and $(PSS/PAH/Eu-POM/PAH)_m$ (bottom) multilayers assembled from 1 M NaCl aqueous solutions for $m = 1-10$. The insets show the peak currents, I (squares), and potentials, E (triangles), of the first redox couple as a function on m (supporting electrolyte, pH 3.0; scan rate, 10 mV/s).

The previous section shows how the surface coverage of POM anions in multilayers can be controlled from submonolayer to multilayer coverage. We anticipate different properties of these layers because the surface coverage will also affect the average cluster spacing and, in turn, the local environment of the POM clusters. In particular, electrochemical experiments have been used to reveal subtle differences in the local environment.[20] In the following section, we will therefore compare the electrochemical properties of two different architectures, namely (a) $(POM/PAH)_m$ and (b) $(PSS/PAH/POM/PAH)_m$ multilayers. The films are adsorbed from dipping solutions containing 1 M NaCl (PAH) and 0.1 M NaCl (POM).

Here, cyclic voltammetry (CV) is used to provide information about POM layer density, permeability, and stability. We note that there is a decrease in the redox current during the first couple of cycles, after which the CVs remain stable. Most likely, loosely bound POM anions may initially diffuse out of the multilayer. In the following, the electrochemical data refer to the fifth CV cycle. Figure 8 shows the CVs of $(Eu-POM/PAH)_m$ and $(PSS/PAH/Eu-POM/PAH)_m$ ($m = 1-10$) multilayers recorded in Eu−POM-free buffer solution at pH 3.0. The surface-confined Eu−POM shows the same redox features as Eu−POM in solution.[3] During the cathodic sweep, three peaks (C1, C2, and C3) occur at potentials of −0.384, −0.466, and −0.522 V, and during the anodic sweep the anodic counterparts (A1, A2, and A3) appear at −0.371, −0.453, and −0.508 V. The three current waves correspond to three $2e^-/2H^+$ redox processes. The peak currents increase linearly with the number of layers, m, for both $(Eu-POM/PAH)_m$ and $(PSS/PAH/Eu-POM/PAH)_m$ multilayers, which confirms linear growth. A plot of the cathodic (I_{pc}) as well as anodic (I_{pa}) peak currents as a function of the scan rate, ν, is linear up to 200 mV/s with zero intercept, and the ratio $I_{pc}(\nu)/I_{pa}(\nu)$ is unity for all scan rates. This result indicates that electron transfer of the surface-confined redox couples is not diffusion limited.[40] The peak currents demonstrate that the amount of redox-active Eu−POM anions is larger in the $(PSS/PAH/Eu-POM/PAH)_m$ multilayers, in agreement with the previous results. Also, in both cases the cathodic peak potential shifts to negative values by approximately 20 mV, while the anodic peak potentials remain almost constant. Obviously, the polyelectrolyte matrix has little influence on the redox kinetics of the Eu−POM centers. The small difference in the anodic and cathodic peak potentials (<40 mV) implies that the redox response remains practically reversible.

The cathodic peak potentials (E_{pc}) shift to negative while the anodic peak potentials (E_{pa}) shift to positive potential when the scan rate increases from 10 to 500 mV/s, which is consistent with a reversible but nonideal redox process. Therefore, we can calculate the surface coverage of Eu−POM anions according to

$$\Gamma = i_p RT[4 - 2\gamma\Gamma]/n^2F^2\nu A \cong i_p RT4/n^2F^2\nu A$$

where i_p is the peak current (amperes), γ is the interaction term, n is the number of electrons transferred per electroactive species, ν is the scan rate (volts per second), A is the geometric area of the electrode (square centimeters), Q is the charge, and all other terms have their usual significance.[41] The analysis of the plot of i_p as a function of ν indicates that $4 \gg 2\gamma\Gamma$.[42] The surface coverage of Eu−POM anions can be directly calculated from the peak current i_p because the polyelectrolyte matrix is not electroactive. The surface coverage of Eu−POM anions per layer amounts to $(1.3 \pm 0.1) \times 10^{-10}$ mol/cm^2 for $(Eu-POM/PAH)_m$ and $(1.7 \pm 0.2) \times 10^{-10}$ mol/cm^2 for $(PSS/PAH/Eu-POM/PAH)_m$ multilayers, respectively. With UV−vis spectroscopy, we determined a surface coverage of 1.8×10^{-10} and 2.0×10^{-10} mol/cm^2, respectively (vide supra). As we noted above, the surface coverage determined with CV is expected to be somewhat lower. We therefore conclude that, within experimental error, the values are in agreement.

We note that the multilayers presented here adhere strongly to different substrates and are stable toward rinsing with water, weak acidic aqueous solution, and organic solvents. An indication of the multilayer integrity is gleaned from successive redox cycling of the surface-immobilized POMs. After 500 double potential steps (−0.6 to 0.8 V), the peak current declines by approximately 8% for the $(Eu-POM/PAH)_{10}$ multilayer but stays practically constant for the $(PSS/PAH/Eu-POM/PAH)_{10}$ multilayer, respectively. We know that Eu−POM does not decompose, even during extensive potential cycling.[3] Therefore, we conclude that the (Eu−POM/PAH) multilayers are more permeable and that Eu−POM may diffuse out of the film under these conditions.

It is interesting to note that the layer architecture also affects the permeability toward electrochemically active probe molecules.[43] Figure 9 shows the electrochemical response of the $Fe(CN)_6^{3-/4-}$ redox probe at electrodes modified with the following multilayers: $(PSS/PAH/Eu-POM/PAH)_{10}$ (solid line,

(39) Israelachvili, J. N. *Intermolecular and Surface Forces*, 2nd ed.; Academic Press: London, 1991.

(40) (a) Oldham, K. B. *J. Electroanal. Chem.* **1981**, *121*, 341. (b) Myland, J. C.; Oldham, K. B. *J. Electroanal. Chem.* **1985**, *182*, 221. (c) Pickup, P. G.; Osteryoung, R. A. *J. Electroanal. Chem.* **1985**, *186*, 99.

(41) Brown, A. P.; Anson, F. C. *Anal. Chem.* **1977**, *49*, 1589.

(42) Smith, D. F.; Willman, K.; Kuo, K.; Murray, R. W. *J. Electroanal. Chem.* **1979**, *95*, 217.

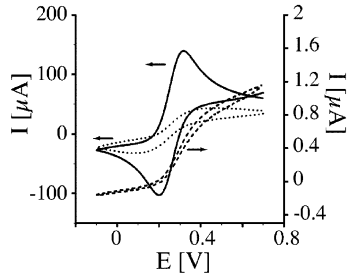

Figure 9. Cyclic voltammograms of $Fe(CN)_6^{3-/4-}$ (5 mM, 1 M KCl) at modified electrodes: (i) solid line, $(PSS/PAH/Eu-POM/PAH)_{10}$ assembled from salt-free solution; (ii) dashed line, $(PSS/PAH/Eu-POM/PAH)_{10}$; (iii) dotted line, $(Eu-POM/PAH)_{10}$ assembled from solutions containing 1 M (PAH) and 0.1 M (POM) NaCl, respectively.

i) assembled from pristine solutions and $(PSS/PAH/Eu-POM/PAH)_{10}$ (dashed line, ii) and $(Eu-POM/PAH)_{10}$ (dotted line, iii) assembled from solutions containing 1 M (PAH) and 0.1 M (POM) NaCl, respectively.

In the first case (i), the redox probe shows a quasi-reversible CV (peak-to-peak separation 100 mV), indicating that the probe diffuses freely through the layer and undergoes electron-transfer reactions at the electrode. In contrast, the same multilayer prepared in the presence of salt (ii) is almost impermeable to the probe molecule. The peak currents decrease by approximately 2 orders of magnitude. Moreover, the CV is broad and plateau-shaped, suggesting current originating from pinholes[44] or strongly hindered diffusion through the multilayer.[45] Similarly, the $(Eu-POM/PAH)_{10}$-coated electrode exhibits broad and plateau-shaped current characteristics, but the peak currents decrease by only a factor of 2 compared to multilayer (i). The fact that the $(Eu-POM/PAH)_{10}$ multilayer is more permeable than in (PSS/PAH/POM/PAH) architecture (ii) is attributed to the extra polyelectrolyte layers, which result in a densely packed, impermeable polyelectrolyte matrix with few defects and pinholes.

Summary and Conclusions

We investigate electrostatic layer-by-layer self-assembly of three discrete nanoscopic POM anions of different sizes and charges with positively charged macromolecules on planar solid surfaces. In all cases, we observe linear and regular multilayer growth. The occurrence of regular growth is consistent with a buildup of an excess interfacial charge by the POM anions, to which the next layer of positively charged polyelectrolyte can bind. Most importantly, the surface coverage of the POM anions can be adjusted from submonolayer to multilayer coverage by adjusting the ionic strength of the dipping solutions. Submonolayer coverage of POM anions, compared to the packing density in the crystalline solid, occurs if no salt is added to the solutions. We propose that residual electrostatic and dipolar repulsions within the interfacial layer keep the surface-confined POM anions separated, thereby reducing the surface coverage. In the presence of salt in the POM dipping solutions, the surface coverage increases to approximately a monolayer. The high ionic strength screens repulsive interactions; thus, the anions can move together more closely. It is interesting to note that at very high ionic strength of the dipping solution, regular film growth may fail, which is in marked contrast to the adsorption of polyelectrolytes. While electrostatic attraction is a prerequisite of multilayer adsorption, two different effects can be identified that may infringe on the conditions for irreversibility: the salt can screen the attractive interactions of the POM anions and the interface, or the entropy gain due to counterion release is not sufficiently high because the concentration of ions in the layer is comparable to that in the solution.[46] Currently, we cannot distinguish the two contributions, but the observation underlines differences in the adsorption of discrete nanoparticles and macromolecular polyelectrolytes. If, in addition, salt is added to the polyelectrolyte dipping solution, the surface coverage increases to approximately two monolayers, which is attributed to penetration of POM anions into the top polyelectrolyte layer. Investigation by AFM reveals a granular surface texture. Adsorption of the discrete nanoscopic POM anions most likely results in an inhomogeneous charge pattern and interfacial reconstruction. Overall, the interfacial roughness of the multilayers remains below or around 1 nm, which we attribute to the annealing effect of the polyelectrolyte.

This study raises the interesting questions of how many charges are required for irreversible adsorption and regular layer growth. The series of POMs that we have investigated so far have 42, 21, 16, 14, and 12 negative charges. In the series of $Co-POM^{16-}$, $Na-POM^{14-}$, and $Eu-POM^{12-}$, we note that the surface coverage is directly related to the number of charges of the anions. Obviously, multiple electrostatic interactions and release of sufficient counterions are required for irreversible adsorption at the polyelectrolyte interface. Other work in our laboratory shows that ions with even fewer charges typically do not adsorb irreversibly unless they are stabilized by additional interactions, such as $\pi-\pi$ stacking.[47] Well-resolved Kiessig fringes in X-ray reflectometry occur only in ELSA films with the two largest POMs. These multilayers are, therefore, homogeneous on a macroscopic length scale. However, no Bragg peaks are observed in these films, indicating the lack of internal structure (stratification). The smaller POMs are probably more dispersed across the interface and also penetrate the polyelectrolyte matrix more easily, thereby reducing the degree of striation. On the basis of this evidence, we suggest that the structure evolves from unstructured films to homogeneous, *striated* layers to high-quality, *stratified* multilayers as the charge and the size of the nanoclusters increase.

On the other side, we can also ask up to which size and charge nanoparticles penetrate into polyelectrolyte multilayers. While small molecules readily diffuse through the entire layer, the smaller POM anions (1−2 nm in diameter) penetrate somewhat, while the larger POM anions (3 nm in diameter) do not penetrate at all into these $PEI(PSS/PAH)_mPSS$ multilayers. This suggests employing POM anions as size-selective probes to study defects, pinholes, and permselectivities in ELSA multilayers.

Cyclic voltammetry demonstrates that the electrochemical properties of POMs are fully maintained in ELSA multilayers. We note that electron transfer of the surface-confined POM

(43) (a) Harris, J. J.; Bruening, M. L. *Langmuir* **2000**, *16*, 2006. (b) Dai, J.; Jensen, A. W.; Mohanty, D. K.; Erndt, J.; Bruening, M. L. *Langmuir* **2001**, *17*, 931. (c) Harris, J. J.; Stair, J. L.; Bruening, M. L. *Chem. Mater.* **2000**, *12*, 1947. (d) Pardo-Yissar, V.; Katz, E.; Lioubashtvski, O.; Willner, I. *Langmuir* **2001**, *17*, 1110. (e) Farbat, T. R.; Schlenoff, J. B. *Langmuir* **2001**, *17*, 1184.
(44) Menon, V. P.; Martin, C. R. *Anal. Chem.* **1995**, *67*, 1920.
(45) Saveant, J.-M. *J. Electroanal. Chem.* **1991**, *302*, 91.
(46) Dubas, S. T.; Schlenoff, J. B. *Macromolecules* **1999**, *32*, 8153.
(47) Krass, H.; Plummer, E. A.; Haider, J. M.; Barker, P. R.; Alcock, N. W.; Pikramenou, Z.; Hannon, M. J.; Kurth, D. G. *Angew. Chem.* **2001**, *113*, 3980; *Angew. Chem., Int. Ed.* **2001**, *40*, 3862.

anions is not diffusion limited and is practically reversible, and that the polyelectrolyte matrix has little influence on the redox kinetics. Within experimental error, the electrochemically determined surface coverage is in agreement with results from UV−vis spectroscopy. Using electrochemically active probe molecules, we note that the permeability of the multilayers can be controlled through the assembly conditions. The probe can freely diffuse through the $(PSS/PAH/Eu-POM/PAH)_{10}$ multilayer prepared at low ionic strength. The same layer prepared at high ionic strength becomes almost impermeable to the probe molecules. Finally, the $(PAH/Eu-POM)_{10}$ multilayer prepared at high ionic strength shows an intermittent permeability. Controlling the permeability through the layer architecture and assembly process is an interesting concept because it allows regulating the access of substrates to the surface-confined POMs. This approach opens a route to implement POM arrays with tailored permselectivities for sensors and catalysts.[48] Finally, we note that, despite the nanoscopic size and discrete charge of POM anions, the final multilayers cannot be washed or rinsed off and also resist extensive electrochemical cycling and application of potential steps.

Acknowledgment. S.L. thanks the Alexander von Humboldt Foundation for a postdoctoral fellowship. The authors are thankful to Helmuth Möhwald for valuable discussions and his support. This work was supported by the Bundesministerium für Bildung und Forschung (BMBF Grant NMT No. 03N8618a/b).

Supporting Information Available: Table of bond distances and angles for the tetranuclear C_4O_{16} unit in the crystal structure of $Na_{16}[Co_4(H_2O)_2(P_2W_{15}O_{56})_2]\cdot 60H_2O$ (PDF); X-ray crystal data for $Na_{16}[Co_4(H_2O)_2(P_2W_{15}O_{56})_2]\cdot 60H_2O$ (CIF). This material is available free of charge via the Internet at http://pubs.acs.org.

JA026946L

(48) Liu, S.; Kurth, D. G.; Volkmer, D. Manuscript in preparation.